GEOLOGICA CARPATHICA, JUNE 2007, 58, 3, 211–228

Fluid induced melting in mantle xenoliths and some implications for the continental lithospheric mantle from the Minusinsk Region (Khakasia, southern Siberia)

ISTVÁN KOVÁCS[1,2], KÁROLY HIDAS[1], JÖRG HERMANN[2], VICTOR SHARYGIN[3], CSABA SZABÓ[1*] and THEODOROS NTAFLOS[4]

[1]Lithosphere Fluid Research Lab, Department of Petrology and Geochemistry, Eötvös University, Pázmány Péter sétány 1/C, H-1117 Budapest, Hungary; *✉ cszabo@elte.hu
[2]Research School of Earth Sciences, The Australian National University, Building 61, Mills Road, Canberra ACT 0200, Australia; istvan.kovacs@anu.edu.au
[3]Institute of Mineralogy and Petrography, United Institute of Geology, Geophysics and Mineralogy, Siberian Branch of Russian Academy of Sciences, Koptuyga Pr. 3, 630090 Novosibirsk, Russia; sharygin@uiggm.nsc.ru
[4]Department of Geological Sciences, Geozentrum, University of Vienna, Althanstrasse 14, A-1090 Vienna, Austria; theodoros.ntaflos@univie.ac.at

(Manuscript received September 12, 2005; accepted in revised form December 7, 2006)

Abstract: Eleven representative xenoliths from the Minusinsk Region, southern Russia were studied in order to highlight the characteristic features of the subcontinental lithospheric mantle beneath the region. Type-I xenoliths show that the lithosphere underwent various degree of depletion overprinted by enrichment processes leading to LREE-enriched pyroxenes. Estimated equilibrium temperature for the xenoliths is in the range of 960–1050 °C. Type-II xenoliths are the result of crystallization from a possibly basaltic melt close to the crust-mantle boundary. Three xenoliths in the Type-I series show evidence of incipient melting such as spongy rims of pyroxenes and interstitial glass. The spongy rims of clinopyroxene consist of clinopyroxene and glass with modal proportion of approximately 82 and 18 %, respectively. Orthopyroxene rim contains olivine (65 %) and glass (35 %) with subordinate amounts of clinopyroxene (< 5 %). Glass within the spongy rims exhibits a clear geochemical affinity to interstitial glass as both have similarly high Al_2O_3, SiO_2 and alkali contents. The interstitial glass and the spongy rims (minerals + glass) display light rare earth (LRE) element and large ion lithophile (LIL) element enriched character. This indicates that incipient melting of pyroxenes occurred in an open system and was likely triggered by the influx of a Na alkali silicate melt/fluid. The interstitial glass represents the residual melt after interaction with the pyroxenes. The formation of this Na-rich silicate melt may represent an earlier stage of the mantle magmatic event that produced the host basalt.

Key words: Minusinsk Region, lithospheric mantle, petrology, major and trace element geochemistry, melting in the upper mantle.

Introduction

Late Cretaceous basaltic volcanic rocks of the North Minusinsk Depression Volcanic Field, southern Russia, (Fig. 1) contain xenoliths both of lower crustal and upper mantle origin, as well as large (up to several cm) clinopyroxene xenocrysts. Earlier studies dealing with the xenoliths of this volcanic field (Ashchepkov et al. 1995; Malkovets et al. 1998, 2000) were focused on a few particular localities (e.g. Tergesh, Krasnoozerskaya, Bele, Kongarovskaya), where garnet-bearing xenoliths (garnet lherzolite and garnet pyroxenite) occur (Malkovets et al. 1998, 2000). Although these papers give detailed studies of the investigated localities, a detailed picture of the lithospheric structure of the North Minusinsk Depression (NMD) has not been established so far. Detailed petrographic and geochemical work on such xenoliths permits us to constrain the nature of the subcontinental mantle.

The modal amount of minerals in xenoliths provides evidence on the degree of depletion and also on enrichment processes acting on a particular mantle region (Frey & Green 1974; Yaxley et al. 1991). Mineral assemblages of the studied mantle xenoliths will be used for highlighting the particular features of the lithosphere beneath the NMD. The composition of the studied pyroxenes allows determination of the *P-T* conditions of the xenoliths, with implications for the thermal state of the lithosphere (Brey & Kohler 1990; Nimis 1995). Furthermore, pyroxene trace element compositions provide an additional tool for exploring multiple depletion and enrichment events (i.e. Ionov et al. 2002).

In this study we present modal contents and major element composition of minerals in seven Type-I and four Type-II xenoliths along with *P-T* estimations. This information is used to gain a better insight into the lithospheric structure of the Minusinsk Region. In the studied series three Type-I xenoliths show signs of incipient melting and contain interstitial glass. In order to better understand this melting event trace and major element analysis of pyroxenes, their rims, interstitial glass and host basalt are presented. We discuss the relationships between glass formed in the rims of pyroxenes with interstitial glass and

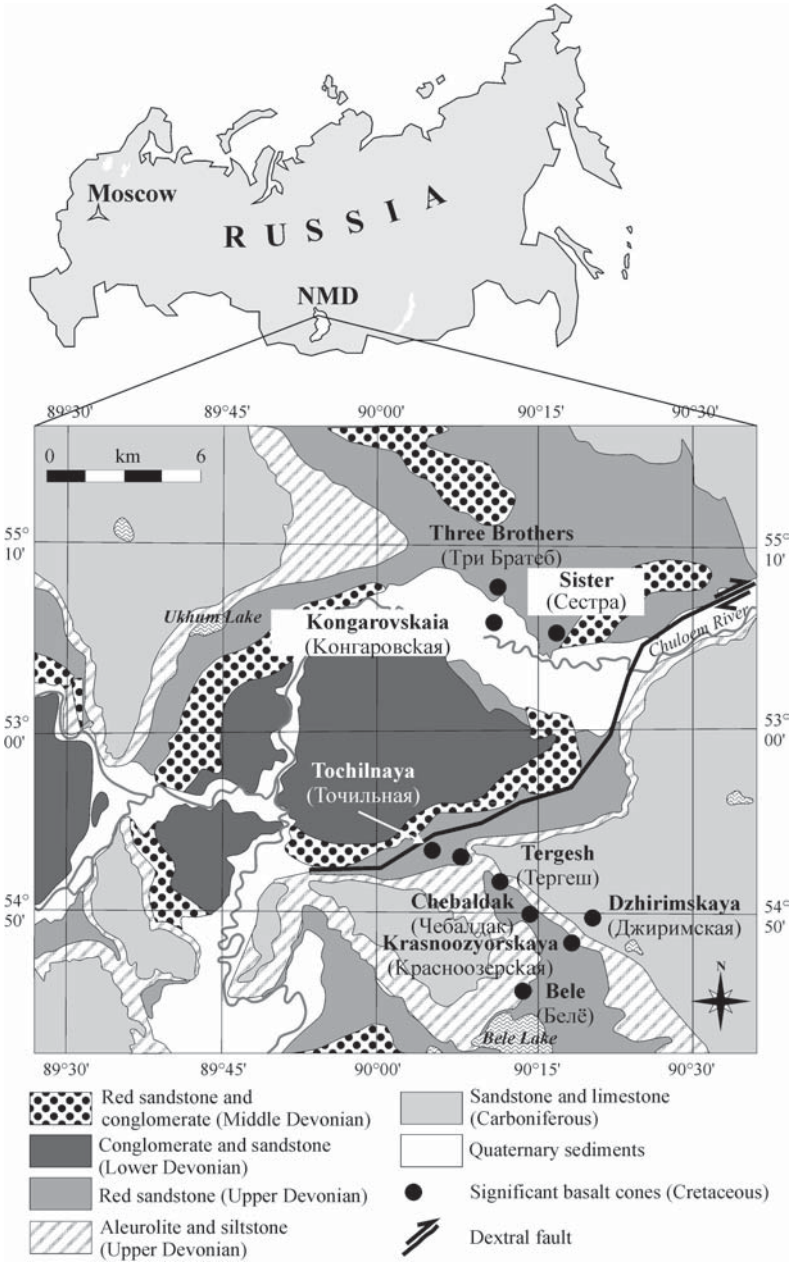

Fig. 1. Schematic geological map of the North Minusinsk Depression showing the most significant basalt pipes (after Malkovets et al. 2003).

with the host basalt. With this data we are able to show that incipient melting was triggered by the influx of an alkaline metasomatic agent that displays chemical affinities to the host basalt.

Geological background

The North Minusinsk Region is located on the Salair segment of the Altay-Sayan fold belt (Fig. 1). The major geological features are trachybasalt-trachyte-trachydacite and basanite-phonotephrite volcanic series erupted in Early to Middle Devonian times (Zubkov 1986; Zonenshain et al. 1990). The genesis of these volcanic series can be related to the formation of a NW-trending Devonian rift system. The area is characterized by a thick Paleozoic sedimentary cover sequence (Fig. 1). Deposition of these sandstones and limestones are presumably related to the Caledonian orogeny. Since then the region has not been affected by any significant tectonic event until the Late Cretaceous when considerable thinning of the lithosphere took place. This thinning is best documented in alkaline basaltic volcanic activity (Zubkov 1986; Zonenshain et al. 1990).

Formation of these Cretaceous basalt pipes began with intensive gas releases and crushing of bedrocks (Kryukov 1964). Then basanitic melts percolated into the axial zone of eruptive breccia and fractures (Luchitsky 1960; Kryukov 1964). Subsequently, these melts reached the surface forming basalt cones along a NW-SE trending vent system (Fig. 1). The northwestern segment of this structure has been moved eastward along a NE-SW trending fault after the Cretaceous (the exact age is unknown). The northern part of the dyke system includes five dykes, whereas the southern group consists of 25 dykes (Fig. 1). The dykes are up to several hundred meters long along strike with a medium thickness of 3–5 m, which locally can reach 10–15 meters. The NW-SE striking dikes are deformed by a number of NE-SW striking dextral strike-slip faults. Such patterns of the volcanic dikes are regarded as evidence for a tangential NE directed extension and a NW directed compression that was coincidental with the penetration of alkali basaltic melt (Ashchepkov et al. 1995).

Formation of the NMD basaltic magmas has been related to decompressional melting of the upwelling asthenospheric material (Litasov et al. 2002). These authors suggested that the driving force for the decompression may have been the geodynamic rearrangement of the Central Asian lithosphere at the onset of the India-Eurasia collision. It is known that the clockwise rotation of the Siberian platform formed local extensional-compressional environments, which led to decompressional melting at greater depths (Khramov 1997).

The age of the basaltic rocks from the Bele and Tergesh (TSH) pipe were determined by the $^{40}Ar/^{39}Ar$ dating technique (Malkovets et al. 2003). They found clearly defined plateau ages of 79 ± 2.0 and 77 ± 1.9 Ma. The $^{40}Ar/^{39}Ar$ ages of 74 ± 5.5 Ma have been found for the Kongarovskaya (KONG) pipe and of 75 ± 6.2 Ma for the Sister (SIST) pipe.

Petrography

In the summer of 2003, 150 mantle xenoliths were collected from eight distinct volcanic pipes of the NMD: Tergesh (TSH) 19, Krasnoozerskaya (KZ) 37, Kongarovskaya (KONG) 33, Three Brothers (BRO) 9, Sister (SIST) 10, Dzhirim (DZH) 19, Chebaldak (CH) 14 and Tochilnaya (TL) 9 (Fig. 1). Eleven samples were selected for detailed studies.

The modal compositions of xenoliths were determined by point counting (at least 2000 points) for each sample (Tables 1 and 2). Two major groups of xenoliths were distinguished. One group consists of peridotite xenoliths containing Cr-diopside (Type-I of Frey & Prinz 1978), in which modal proportion of olivines always exceeds 40 vol. %. Seven Type-I xenoliths (CHI3, DZH1, KZC1, KZSI6, SISTI2b, TLC1, TSHII9) have been studied. The other group includes four xenoliths (BROI1, KONGII1, KZSII4, SISTII5) and is characterized by a high modal proportion of pyroxenes (orthopyroxene + clinopyroxene > 80 v/v %) and the presence of Al-augite (Type-II, of Frey & Prinz 1978).

Type-I xenoliths

The peridotite xenoliths include: three wehrlites (SISTI2b, CHI3, DZH1), two lherzolites (KZC1, TSHII9), one harzburgite (TLC1) and one dunite (KZSI6) (see their modal composition in Tables 1 and 2). The xenoliths usually exhibit porphyroclastic texture, however, protogranular texture also occurs subordinately. The grain boundaries are slightly curved, and internal strain features are absent, or occur only rarely in the large porphyroclasts (olivines and mostly orthopyroxenes).

Primary olivine (ol-1) is often found as porphyroclasts (up to 3.5 mm) or smaller anhedral crystals (0.5–1.0 mm). The grain boundaries are straight (Fig. 2a and 2b). Newly formed (secondary) olivine (ol-2), is found only in rare spongy rims of orthopyroxene (details below, Fig. 2c and 2d). Such newly formed olivine is elongated and radial to orthopyroxene and has an average grain size of less than 80 μm.

Primary clinopyroxene (cpx-1) is present as fine-grained crystals with an average grain size of 0.5–1.0 mm. The grain boundaries are curved and in several peridotites the clinopyroxene has a spongy rim, which consists of clinopyroxene and glass. The clinopyroxene core is always clear (Fig. 2a). The proportion of the spongy clinopyroxene and the glass was calculated using backscattered electron (BSE) images, and it gives consistently 82–88 % area for the spongy clinopyroxene and 12–18 % area for the enclosed glass (Fig. 2a and 2b).

Orthopyroxene (opx-1) is frequently observed as porphyroclasts (up to 4 mm). Orthopyroxene occasionally has a spongy rim, which contains small olivine grains and glass (Fig. 2c and 2d). The proportions of olivine (ol-2) and glass are 65 % area and 35 % area, respectively. However, rare newly formed clinopyroxene (cpx-2) was also recognized in spongy rims (max. 5 % area) (Fig. 2d). Generally, the spongy rim around orthopyroxene is less extensive than the spongy rim around clinopyroxene. Primary spinel (sp-1) occurs as isometric relatively small (0.5–1.0 mm), brown coloured grains mostly in interstitial settings. Occasionally, it can be found as inclusions within silicate phases. Some spinel rarely contains spongy rims, as well. Spinel was also identified as dark brown lamellae in clinopyroxene (sp-1) (DZH1 wehrlite (Fig. 2e) and KZC1 lherzolite). Secondary spinel (sp-2) was only found in interstitial glass of SISTI2b wehrlite (details below), with a grain size of 20–40 μm.

Interstitial glass (i.e. not only along grain boundaries) was found in the wehrlite SISTI2b as amorphous brown coloured patches ranging in size from 250 to 300 μm. The modal proportion of the glass is considerable (2.4 v/v %). The interstitial glass is not homogeneous and includes secondary clinopyroxene (< 200 μm), spinel (20–40 μm) and feldspar (< 200 μm) crystals. Minor interstitial glass patches were also recognized in KZC1 lherzolite, however, detailed petrographic observation was not possible due to the small size of the glass inclusions (< 100 μm). Glass was also identified along the rims of spongy clinopyroxenes and orthopyroxenes (SISTI2b wehrlite, TLC1 harzburgite, KZC1 lherzolite).

Type-II xenoliths

Pyroxenite-rich xenoliths (Type-II) are clinopyroxenites (KONGII1; SISTII5), plagioclase-bearing ultramafic rock (KZSII4) and olivine websterite (BROI1) (Table 2). These rocks display an igneous texture. Tiny elongated spinel lamellae frequently occur in clinopyroxenes. In addition, oriented amphibole lamellae can also be observed (KONGII1 clinopyroxenite), and slightly altered amphibole patches are also present. Plagioclase was only found in one xenolith (KZSII4 clinopyroxenite). Vermicular green spinel inclusions were recognized in this plagioclase (Fig. 2f).

Geochemistry

Analytical techniques

Major element compositions of the primary minerals were determined with a JEOL SUPERPROBE JXA-8600 electron microprobe at the Department of Earth Sciences, University of Florence, Italy. The operating conditions were: accelerating voltage of 15 kV, beam current of 10 nA, beam size of 5 μm for pyroxene and spinel, 3 μm for amphibole and feldspar, and 40 s of counting time for all the elements. Standard corrections of Bence & Albee (1968) were applied.

The compositions of glass and minerals affected by melting (i.e. spongy clinopyroxene, incongruent orthopyroxene and interstitial glass) were obtained by wavelength-dispersive spectrometry using a CAMECA SX-100 electron probe X-ray microanalyser at the Department of Geological Sciences, University of Vienna, Austria. Operating conditions were: accelerating voltage of 20 kV, beam current 10 nA with a beam size 5 μm. Only glassy patches bigger than 10 μm were considered for analysis, in

Table 1: Major (wt. %), trace element (ppm) and modal (vol. %) compositions of minerals of KZC1 (spinel lherzolite), SISTI2b (wehrlite) and TLC1 (harzburgite). Host basalt analysis is also indicated. *Continued on the next page.*

ZC1 (lherzolite), ol = 44.9, opx = 18.6, cpx = 33.5, sp = 3

Mineral	**ol***	**opx**	**cpx**	**sp**	**spongy cpx**			**spongy opx**			**interstitial glass**
					cpx	**glass**	**bulk****	**cpx**	**glass**	**bulk*****	
No.	**2**	**2**	**2**	**2**	**7**	**11**	**(±2%)**	**4**	**4**	**(±10%)**	**2**
SiO_2	40.86	56.13	53.02	0.03	52.90	60.42	53.88	54.20	64.72	49.33	62.73
TiO_2	n.a.	0.09	0.26	0.12	0.56	0.22	0.52	0.43	0.22	–	0.25
Al_2O_3	n.a.	4.43	5.96	56.04	2.74	21.10	5.13	1.18	17.57	–	21.55
Cr_2O_3	n.a.	0.35	0.68	11.03	1.01	n.d.	–	1.18	0.00	–	0.00
FeO_{tot}	9.81	6.26	3.09	11.98	2.80	0.95	2.56	3.31	1.34	6.80	0.71
MnO	0.15	0.13	0.11	0.13	0.10	0.03	0.09	0.14	0.02	0.11	0.00
NiO	0.37	0.06	n.a.	0.35	n.a.	n.d.	–	n.a.	0.00	0.24	0.00
MgO	49.31	33.02	15.50	20.09	17.80	1.87	15.73	18.90	1.83	32.45	0.83
CaO	0.05	0.69	20.27	0.01	21.70	4.98	19.53	20.70	0.36	0.16	3.27
Na_2O		0.13	1.32	0.14	0.58	7.09	1.43	0.58	6.35	2.26	8.04
K_2O		0.00	n.d.	0.00	0.01	1.64	0.22	0.00	5.99	2.13	2.00
P_2O_5						0.13	0.02		0.08	0.03	0.10
BaO						0.09	0.01		0.03	0.01	0.07
SrO						0.10	0.01		0.00	0.00	0.02
SO_2						n.d.	–		0.02	0.01	0.01
Cl						0.01	0.00		0.01	0.00	0.01
Total	100.36	101.18	100.19	99.69	100.20	98.62		100.70	98.56		99.60
mg#	0.90	0.88	0.87	0.70	0.90	0.73		0.89	0.65		0.62
mg# (cpx****)						0.93			0.90		0.88
											basalt
No.	**2**	**3**	**2**								**2**
Int. std.	SiO_2	SiO_2	SiO_2								SiO_2=52
Li	2.7	3.5	7.4								6.2
Be	0.006	0.056	0.13								1.8
B	6.0	5.7	4.5								6.1
P	47	62	47								7830
Sc	3.2	18	70								6.1
Ti	21	493	1990								3720
V	3.1	95	257								27
Co	138	59	22								5.9
Rb	0.057	0.017	0.067								23
Sr	0.21	0.76	86								1600
Y	0.036	0.77	14								18
Zr	0.18	0.20	3.3								120
Nb	0.090	0.038	0.79								66
Cs	n.d.	0.004	0.003								0.32
Ba	0.54	0.11	0.94								496
La	0.054	0.016	8.0								68
Ce	0.082	0.028	8.4								114
Pr	0.013	0.003	0.62								12
Nd	0.043	0.016	2.2								44
Sm	n.d.	0.010	0.81								7.6
Eu	n.d.	0.005	0.36								2.5
Gd	n.d.	0.030	1.5								6.2
Tb	0.001	0.008	0.30								0.77
Dy	n.d.	0.089	2.3								4.2
Ho	0.002	0.028	0.53								0.72
Er	0.008	0.12	1.6								1.8
Tm	0.002	0.025	0.24								0.22
Yb	0.015	0.22	1.6								1.3
Lu	0.004	0.041	0.23								0.17
Hf	0.006	0.015	0.28								2.5
Ta	0.006	0.001	0.029								3.3
Pb	0.010	0.010	1.1								2.6
Th	0.020	0.012	1.9								7.4
U	0.009	0.012	0.57								1.9

Explanations to abbreviations see on the next page.

Table 1: *Continued.*

SISTI2b (wehrlite), ol = 83, opx = 0.6, cpx = 14, glass = 2.4

Mineral	ol*	opx	cpx	spongy cpx			spongy opx			interstitial glass			
				cpx	glass	bulk**	cpx	glass	bulk***	glass	cpx****	fdp****	sp****
No.	6	1	1	13	4	(±16 %)	2	4	(±10 %)	10	6	8	5
SiO_2	40.76	55.95	52.70	50.80	57.54	51.84	55.20	58.47	47.04	54.78	48.70	57.10	0.67
TiO_2	0.01	0.08	0.23	0.94	0.27	0.84	0.16	0.78	0.28	1.65	1.62	0.21	3.36
Al_2O_3	0.03	2.92	3.19	4.86	25.56	8.07	0.57	23.04	8.20	23.27	6.51	26.70	32.60
Cr_2O_3	0.01	0.31	1.21	1.31	0.04	1.11	0.62	0.01	0.01	0.02	1.75	0.02	26.20
FeO_{tot}	11.57	6.72	3.38	3.52	0.30	3.02	3.23	0.82	7.76	1.34	3.54	0.28	19.90
MnO	0.19	0.20	0.12	0.09	0.00	0.08	0.13	0.01	0.13	0.02	0.07	0.01	0.18
NiO	0.30	n.a.	n.a.	n.a.	0.01	–	n.a.	0.00	0.19	0.01	n.a.	0.00	0.27
MgO	47.61	32.24	16.66	16.60	0.29	14.07	19.60	0.45	30.87	0.82	15.40	0.06	15.80
CaO	0.09	0.77	21.65	21.90	8.53	19.83	21.30	0.37	0.19	0.77	22.50	8.47	0.06
Na_2O		0.50	0.50	0.63	6.33	1.51	0.59	8.26	2.93	8.27	0.65	6.28	0.12
K_2O		0.15	0.02	0.01	0.69	0.12	0.01	4.07	1.44	3.92	0.02	0.67	0.06
P_2O_5					n.d.			0.12	0.04	0.44		0.04	
BaO					n.d.			0.08	0.03	0.05		0.05	
SrO					n.d.			n.d.	–	0.06		0.08	
SO_2					n.d.			0.02	0.01	0.02			
Cl					n.d.			0.14	0.05	0.19			
Total	100.58	99.84	99.67	100.70	99.56		101.40	96.64		95.62	100.80	100.04	99.20
mg#	0.88	0.87	0.87	0.87	0.57		0.89	0.43		0.46	0.86		0.52
mg# (cpx*****)					0.86			0.74		0.79			

			measured		basalt
No.	8	1	8	7	4
Int. std.	SiO_2	SiO_2	SiO_2	SiO_2	SiO_2=52
Li	5.0	20	4.6	29	12
Be	0.05	0.32	0.32	5.5	2.2
B	9.2	8.0	7.4	15	8.0
P	163	125	137	3320	8560
Sc	4.3	53	53	5.8	23
Ti	79	821	1500	11700	14900
V	9.3	160	169	50	145
Co	118	22	19	4.9	38
Rb	0.14	0.024	3.6	108	28
Sr	0.39	267	173	273	1530
Y	0.18	14	16	21	25
Zr	1.6	195	240	520	233
Nb	0.047	0.67	3.4	362	95
Cs	0.008	n.d.	0.28	2.3	0.65
Ba	0.10	0.14	51	388	682
La	0.015	9.4	11	59	70
Ce	0.027	30	35	119	126
Pr	0.009	4.5	5.4	12	14
Nd	0.053	22	26	45	55
Sm	0.048	5.2	6.1	7.7	10
Eu	0.014	1.7	2.5	1.2	3.5
Gd	0.070	4.8	5.4	6.2	8.7
Tb	0.011	0.63	0.72	0.83	1.1
Dy	0.06	3.5	4.0	4.7	6.0
Ho	0.014	0.56	0.66	0.81	0.99
Er	0.033	1.32	1.6	2.1	2.4
Tm	0.007	0.16	0.20	0.28	0.30
Yb	0.038	0.95	1.2	1.7	1.8
Lu	0.007	0.13	0.16	0.23	0.25
Hf	0.071	4.2	4.9	8.6	5.2
Ta	0.003	0.08	0.22	17	4.8
Pb	0.012	0.28	0.26	4.7	5.0
Th	n.d.	0.30	0.44	13	7.9
U	0.02	0.066	0.09	3.6	2.0

n.d. — not detected; n.a. — not analysed; mg# — $Mg/(Mg+Fe_{tot})$; * — composition represents both primary and newly formed olivines (in spongy rim of orthopyroxene); ** — calculated bulk composition using 23.5 % glass and 76.5 % cpx, error arises from the area measurements; *** — calculated bulk composition using 64.5 % olivine and 35.5 % glass, cpx is excluded since its modal contribution is negligible; **** — calculated mg# of clinopyroxene in equilibrium with glass, using the partition coefficient of Draper & Green (1997).

Table 1: *Continued from the previous pages.*

TLC1 (harzburgite), ol = 62.2, opx = 33.7, cpx = 1.7, sp = 2.4

Mineral	**ol***	**opx**	**cpx**	**sp**	**spongy cpx**			**spongy opx**		
					cpx	**glass**	**bulk****	**cpx**	**glass**	**bulk*****
No.	**2**	**2**	**1**	**3**	**5**	**6**	**(±7%)**	**8**	**4**	**(±10%)**
SiO_2	40.90	56.00	53.03	0.07	53.70	65.29	56.42	54.40	65.21	49.53
TiO_2	0.00	0.10	0.29	0.16	0.51	0.65	0.54	0.25	0.39	0.14
Al_2O_3	0.08	5.07	6.63	54.13	1.64	18.37	5.57	0.83	18.34	6.56
Cr_2O_3	0.03	0.45	0.81	13.29	1.22	0.02	0.94	1.26	0.02	0.02
FeO_{tot}	9.85	6.25	3.57	12.02	2.84	0.61	2.32	2.94	0.84	6.65
MnO	0.15	0.13	0.14	0.14	0.12	0.01	0.09	0.12	0.02	0.10
NiO	0.33	n.a.	n.a.	0.33	n.a.	0.01	–		0.02	0.22
MgO	49.22	32.23	16.15	19.90	18.50	0.47	14.26	19.70	0.84	32.04
CaO	0.12	1.01	18.86	n.d.	21.40	0.48	16.48	19.90	0.16	0.13
Na_2O		0.11	1.34	n.a.	0.74	7.20	2.26	0.77	6.01	2.13
K_2O		0.01	0.02	n.a.	0.05	5.57	1.35	0.05	5.94	2.11
P_2O_5						0.04	0.01		0.07	0.02
BaO						0.01	0.00		0.03	0.01
SrO						n.d.	–		n.d.	–
SO_2						0.01	0.00		0.02	0.01
Cl						n.d.	–		0.03	0.01
Total	100.66	101.34	100.84	100.05	100.70	98.70		100.20	97.96	
mg#	0.90	0.88	0.86	0.70	0.90	0.51		0.90	0.58	
mg# (cpx****)						0.83			0.86	

				measured		measured	basalt
No.	**2**	**4**	**3**	**2**		**5**	**3**
Int. std.	SiO_2	SiO2	SiO_2	SiO_2		SiO_2	SiO_2=52
Li	4.3	2.3	10	5.9		7.2	11
Be	n.d.	0.056	0.13	0.47		0.20	2.8
B	4.9	5.1	4.2	6.6		14	9.5
P	266	25	152	803		269	8615
Sc	4.3	19	58	54		22	21
Ti	45	605	1960	4310		1030	13300
V	7.3	104	239	233		109	119
Co	141	63	26	46		67	31
Rb	0.059	0.043	0.14	17		26	43
Sr	0.72	2.3	533	472		93	1230
Y	0.12	1.1	14	15		3.1	27
Zr	0.20	0.81	7.9	37		5.4	210
Nb	0.10	0.24	3.7	23		5.7	139
Cs	n.d.	n.d.	0.013	0.37		0.25	0.89
Ba	0.39	0.20	1.9	130		66	702
La	0.044	0.13	34	28		6.1	86
Ce	0.10	0.49	80	68		14	145
Pr	0.007	0.044	5.6	5.92		1.2	15
Nd	0.041	0.14	14	19		3.8	56
Sm	n.d.	0.037	2.0	3.2		0.64	10.0
Eu	n.d.	0.016	0.66	1.0		0.30	3.2
Gd	n.d.	0.071	2.2	3.1		0.58	8.3
Tb	n.d.	0.015	0.35	0.46		0.087	1.1
Dy	0.017	0.15	2.5	3.0		0.58	6.0
Ho	0.004	0.041	0.52	0.60		0.12	1.0
Er	0.018	0.16	1.5	1.7		0.36	2.7
Tm	0.004	0.029	0.22	0.23		0.055	0.34
Yb	0.031	0.26	1.4	1.5		0.41	2.1
Lu	0.008	0.045	0.20	0.21		0.06	0.29
Hf	n.d.	0.028	0.33	0.87		0.11	4.3
Ta	0.008	0.006	0.15	0.93		0.17	5.8
Pb	0.033	0.016	0.36	0.82		0.44	8.1
Th	0.011	0.017	1.7	2.6		0.51	12
U	n.d.	0.008	0.25	0.55		0.14	3.0

n.d. — not detected; n.a. — not analysed; mg# — $Mg/(Mg+Fe_{tot})$; * — composition represents both primary and newly formed olivines (in spongy rim of orthopyroxene); ** — calculated bulk composition using 23.5 % glass and 76.5 % cpx, error arises from the area measurements; *** — calculated bulk composition using 64.5 % olivine and 35.5 % glass, cpx is excluded since its modal contribution is negligible; **** — calculated mg# of clinopyroxene in equilibrium with glass, using the partition coefficient of Draper & Green (1997).

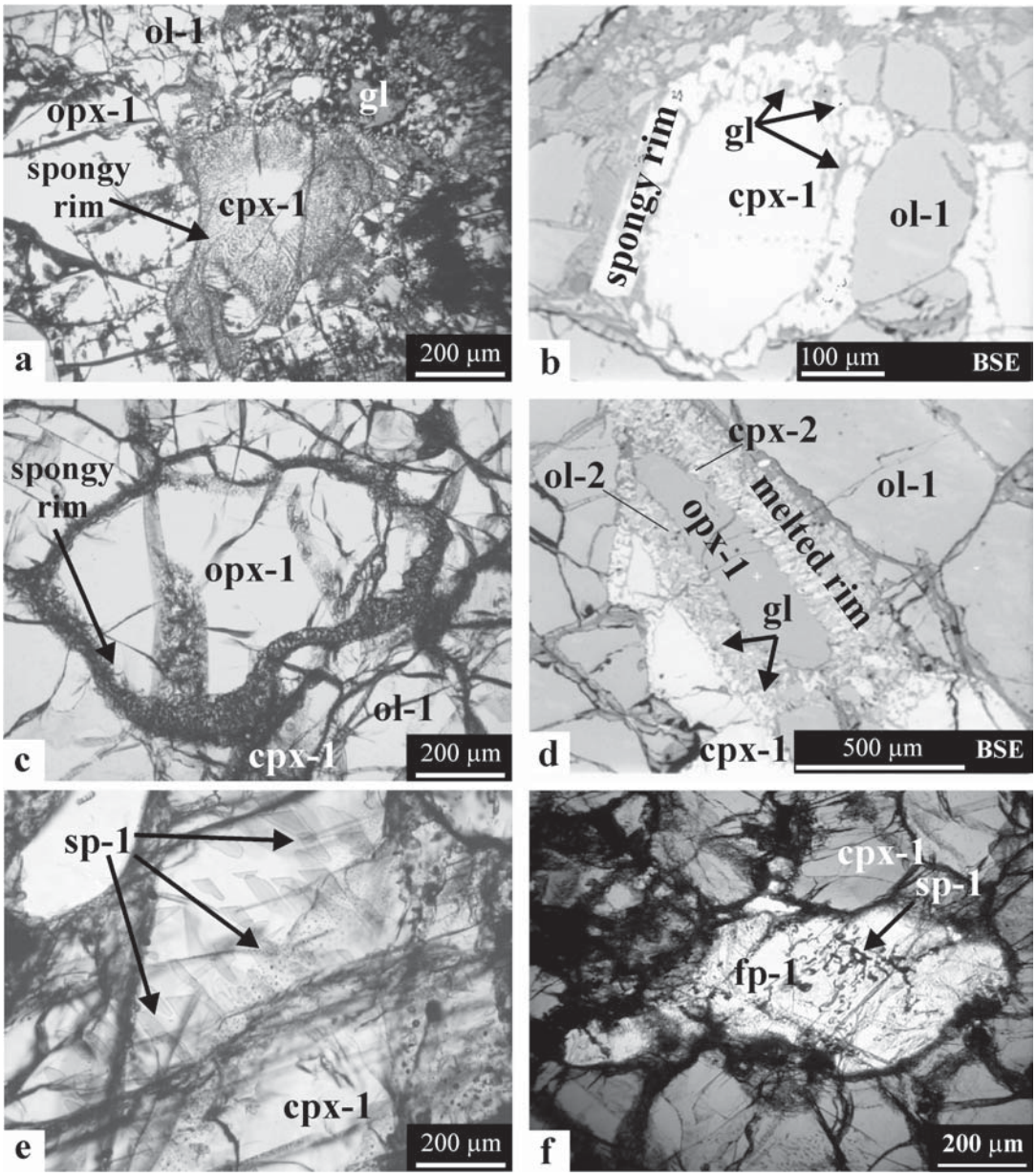

Fig. 2. Photomicrographs of fabrics and textural features in the North Minusinsk Depression upper mantle xenoliths. Photos (a), (c), (e) and (f) were taken in plane polarized light. Photos (b) and (d) are BSE images. **cpx-1** — clinopyroxene core; **cpx-II** — newly formed clinopyroxene relating to the spongy rim of orthopyroxene; **fp-1** — feldspar; **gl** — glass; **ol-1** — olivine; **ol-II** — newly formed olivine relating to the spongy rims of orthopyroxene; **opx-1** — orthopyroxene; **sp-1** — spinel. **(a)** — Melting of clinopyroxene (SISTI2b wehrlite) surrounded by primary olivine. **(b)** — Melted (spongy) clinopyroxene on BSE image (KZC1 lherzolite) surrounded by primary olivine. **(c)** — Incongruent melting of orthopyroxene (TLC1 harzburgite). Orthopyroxene breaks down into fine-grained assemblages of clinopyroxenes, olivine and glass. **(d)** — BSE image of a melted orthopyroxene in KZC1 lherzolite. **(e)** — Spinel found as dark-brown lamellae in clinopyroxene (DZH1 wehrlite and KZC1 lherzolite). **(f)** — Vesicular, green spinel inclusions were recognized in plagioclase (KZSII4 clinopyroxenite).

order to avoid significant volatilization. Potential volatilization and loss of Na and K was monitored via plotting the count rates as a function of counting time. Corrections have been made where it was necessary. Counting times for Na and K were 10 seconds and for all other elements 40 seconds with standard ZAF correction procedures applied.

Trace element composition of interstitial glass, host basalt, and minerals were measured by laser ablation, inductively-coupled plasma mass spectrometry (LA ICP-MS) at the Research School of Earth Sciences, Australian National University, Australia. A pulsed 193 nm ArF Excimer laser with 100 mJ energy at a repetition rate of 5 Hz coupled to an Agilent 7500 quadropole ICP-MS were used for ablation. A spot size of 180 μm was needed for silicate phases and host basalt, and a size of 80 μm was deployed for interstitial glass. From the spongy rim of clinopyroxene and incongruent rim of orthopyroxene only bulk analyses were available, due to the grain sizes of secondary miner-

Table 2: Major element (wt. %) and modal composition (vol. %) of minerals from additional representative Type-I and Type-II Minusa xenoliths.

KZSI6 (dunite)				TSHII9 (lherzolite)				CHI3 (wehrlite)				DZH1 (wehrlite)			
ol = 90.8, opx = 4.5*, cpx = 1.6, sp = 3.1				ol = 66.2, opx = 15.1, cpx = 14.5, sp = 4.2				ol = 79.8, opx = 2.9, cpx = 15.5, sp = 1.8				ol = 48.2, opx = 2, cpx = 48.2, sp = 1.6			
Mineral	**ol**	**cpx**	**sp**	**ol**	**opx**	**cpx**	**sp**	**ol**	**opx**	**cpx**	**sp**	**ol**	**opx**	**cpx**	**sp**
No.	**3**	**2**	**3**	**2**	**3**	**3**	**3**	**4**	**2**	**2**	**2**	**2**	**2**	**2**	**2**
SiO_2	40.72	53.49	0.01	41.82	55.19	53.27	0.04	41.00	55.81	53.67	0.07	40.7	56.81	53.79	0.04
TiO_2	n.a.	0.23	0.19	n.a.	0.11	0.41	0.20	0.01	0.03	0.11	0.08	n.a.	0.07	0.16	0.145
Al_2O_3	n.a.	4.40	42.48	n.a.	5.08	6.81	54.49	0.03	3.81	4.85	49.27	n.a.	3.22	4.12	45.59
Cr_2O_3	n.a.	0.66	23.16	n.a.	0.55	0.87	14.12	0.02	0.44	1.07	17.86	n.a.	0.33	0.64	20.41
FeO_{tot}	12.15	3.25	18.03	9.19	5.98	3.02	11.05	10.99	6.90	3.52	14.08	9.39	6.48	3.00	15.26
MnO	0.19	0.10	0.18	0.17	0.14	0.09	0.09	0.19	0.22	0.13	0.16	0.14	0.10	0.10	0.19
NiO	0.29	n.a.	0.21	0.34	n.a.	n.a.	0.31	0.32	n.a.	n.a.	0.29	0.26	n.a.		0.35
MgO	47.25	15.32	16.03	49.60	32.57	15.76	20.00	48.49	32.87	15.86	18.82	48.9	33.39	16.24	18.27
CaO	0.05	21.05	n.d.	0.11	0.91	18.87	0.02	0.09	0.69	18.83	0.01	0.06	0.65	21.18	0.04
Na_2O		1.36	n.a.		0.22	1.57	0.00		0.18	1.74	n.a.		0.07	0.99	0.05
K_2O		0.02	n.a.		n.a.	n.d.	n.a.		0.01	n.d.	n.a.		0.03	n.d.	0.02
Total	100.65	99.85	100.38	101.22	100.71	100.67	100.34	101.14	100.93	99.75	100.76	99.33	101.13	100.19	100.01
mg#	0.87	0.87	0.55	0.91	0.88	0.88	0.71	0.89	0.87	0.86	0.65	0.90	0.88	0.88	0.62
cr#			0.27				0.15				0.20				0.23

BROI1 (olivine websterite)				KONGII1 (clinopyroxenite)				SISTII5 (clinopyroxenite)			KZSII2 (plagioclase b. ultramafic rock)		
ol = 6, opx = 23, cpx = 69, sp = 2				cpx = 83.2, opx = 3.3, sp = 1.3, amph = 12.2				cpx = 85, sp = 13, glass = 2			cpx = 91.6, sp = 4.8, fdp = 3.6		
Mineral	**ol**	**opx**	**cpx**	**sp**	**cpx**	**opx**	**sp**	**cpx**	**sp**	**glass**	**cpx**	**sp**	**fdp**
No.	**1**	**3**	**3**	**1**	**2**	**2**	**2**	**1**	**1**	**1**	**2**	**3**	**2**
SiO_2	41.7	56.5	54.1	0.02	52.2	55.1	0.02	44.4	0.04	52.07	46.30	0.03	52.14
TiO_2	n.a.	0.08	0.15	0.13	0.70	0.15	0.16	1.39	0.34	n.d.	1.51	0.09	0.03
Al_2O_3	n.a.	3.29	4.23	40.65	6.09	4.35	61.4	13.6	54.2	30.88	11.85	61.15	30.68
Cr_2O_3	n.a.	0.47	1.22	25.71	0.09	0.06	2.78	n.d.	0.03		n.d.	0.05	0.00
FeO_{tot}	10.3	5.32	3.25	14.80	4.93	10.2	19.6	9.14	32.8	0.75	7.46	25.86	0.10
MnO	0.21	0.20	0.14	0.21	0.13	0.17	0.21	0.11	0.27	0.03	0.07	0.30	0.01
NiO	n.a.	0.08	n.a.	n.a.		n.a.	0.30	n.a.	n.a.	n.a.	n.a.	n.d.	
MgO	48.5	33.0	16.3	15.93	14.6	30.55	17.0	8.88	12.8	0.06	10.32	13.86	0.03
CaO	0.07	0.70	20.8	0.02	21.4	0.62	0.01	20.8	0.08	13.14	21.20	0.03	12.80
Na_2O		0.05	0.91	n.d.	0.79	0.07	n.a.	1.56	0.04	3.44	1.24	0.07	3.77
K_2O		n.d.	n.d.	0.03	0.01	0.03	n.a.	n.d.	0.02	0.29	n.d.	0.01	0.15
Total	100.75	99.60	101.02	97.50	100.88	101.28	101.62	99.83	100.47	100.68	99.93	101.60	99.68
mg#	0.89	0.90	0.87	0.60	0.80	0.81	0.55	0.57	0.35		0.66	0.43	
cr#				0.30			0.03		0.00			0.00	

n.d. — not detected, n.a.— not analysed, mg# — Mg/(Mg+Fetot), cr# — Cr/(Cr+Al)
* Major element analysis of orthopyroxene was not possible

als and glass patches which were much less than the optimal smallest spot size. The counting time was 20–25 s for the background and 40–45 s for sample analysis. Instrument calibration was against NIST 612 glass, and NIST 610 and BCR glass were used as secondary standards. ^{29}Si was employed as the internal standard isotope, based on SiO_2 concentrations previously measured by electron microprobe. For the spongy rims of pyroxenes SiO_2 concentrations from the calculated mass balance were used as internal standards (see below) (Table 1).

Major element composition

Olivine

Regardless of their textural setting (primary ol-1 or newly formed ol-2 in spongy rim of orthopyroxene) olivines from the NMD xenoliths have similar major element compositions and display a narrow compositional range. Mg-values (mg#) range from 0.87 to 0.91 (Tables 1 and 2). Olivine in the dunite xenolith (KZSI6) shows the lowest values, whereas olivine in TSHII9 lherzolite displays the highest forsterite content. There is no significant variation between Type-I and Type-II xenoliths in terms of mg#. The NiO content is in the range of 0.26–0.37 wt. % in the Type-I series. Only BROI1 (olivine websterite) of the Type-II group contains olivine, but this has not been analysed for NiO (Table 2).

Orthopyroxene

Orthopyroxene (opx-1) has a different composition in the Type-I and olivine websterite (BROI1) xenoliths. Orthopyroxene in lherzolites, harzburgites has more Al_2O_3 (4.4–5.7 wt. %) than in wehrlites and olivine websterite (2.9–3.8 wt. %) (Tables 1 and 2). Orthopyroxene in Type-I series and olivine websterite (BROI1) is characterized by approximately 88–90 En component, 0.30–0.50 wt. % of Cr_2O_3 and maximum 0.11 wt. % of TiO_2 contents. In contrast, orthopyroxenes in Type-II xenoliths (KONGII1) of the NMD have lower Cr_2O_3 (0.06 wt. %) and slightly elevated TiO_2 content (0.15 wt. %) than the orthopyroxenes in the Type-I series (Table 2).

Clinopyroxene

Primary clinopyroxenes (cpx-1) in the Type-I xenoliths has 3.19–6.81 wt. % of Al_2O_3 (Tables 1 and 2). Clinopyroxene in harzburgite and lherzolites has more TiO_2 and Al_2O_3 (0.26–0.41 wt. %, 5.96–6.81 wt. %, respectively) than in wehrlites and olivine websterite (0.11–0.23 wt. %, 3.19–4.85 wt. %, respectively). The Na_2O- and Al_2O_3-content of clinopyroxene shows scattered distribution. FeO and TiO_2 display narrower compositional range and also negative correlation with MgO.

The major element composition of the newly formed clinopyroxene (cpx-2) varies with its textural setting (Table 1, Fig. 3). The clinopyroxene incorporated in interstitial glass is rich in Al_2O_3 (5.90–7.67 wt. %), TiO_2 (1.42–2.36 wt. %) and Cr_2O_3 (0.82–2.98 wt. %) and poor in MgO (14.6–15.9 wt. %) and SiO_2 (47.6–49.1 wt. %). In spongy rims of orthopyroxene, it is rich in SiO_2 (53.7–55.2 wt. %), MgO (18.7–20.4 wt. %) and Cr_2O_3 (0.51–1.66 wt. %), but poor in Na_2O (0.57–0.87 wt. %) and Al_2O_3 (0.47–1.28 wt. %). The spongy rims of primary clinopyroxene (cpx-1) possess low Na_2O (0.36–1.30 wt. %), Al_2O_3 (0.58–3.81 wt. %) and high Cr_2O_3 (0.46–2.26 wt .%) and CaO (19.9–22.8 wt. %) contents (Fig. 3).

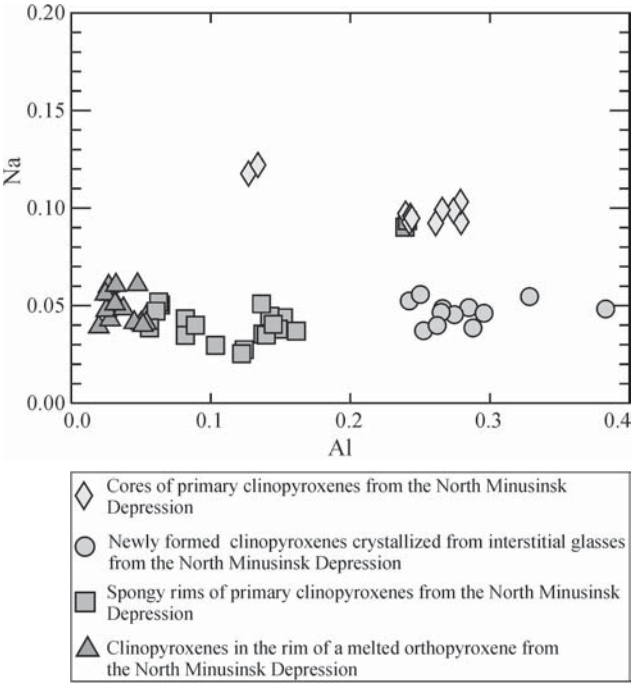

Fig. 3. Na vs. Al (in a.p.f.u.) diagram for clinopyroxenes from different textural setting in the North Minusinsk Depression xenoliths which exhibit evidence of melting/metasomatism (KZC1 lherzolite, SISTI2b wehrlite, TLC1 harzburgite).

In the Type-II xenoliths the clinopyroxene has 44.4–54.1 wt. % of SiO_2, 8.91–16.3 wt. % of MgO and 4.20–13.6 wt. % of Al_2O_3. Clinopyroxene, especially in clinopyroxenite- and plagioclase-bearing ultramafic xenoliths (KZSII1, SISTII5) show considerably lower amounts of SiO_2 and MgO, whereas, they are enriched in Al_2O_3 (Table 2). Clinopyroxene in KZSII1 clinopyroxenite and SISTII5 plagioclase-bearing ultramafic xenoliths is distinct from that in the BROI1 olivine websterite and KONGII1 clinopyroxenite (Table 2).

Spinel

Primary spinel (sp-1) in Type-I xenoliths has 11.0–23.2 wt. % of Cr_2O_3, 42.5–56.0 wt. % of Al_2O_3 and mg# of 0.61–0.76 (Tables 1 and 2). Newly formed spinel (sp-II in the interstitial glass of SISTI2b wehrlite) has a 23.3–30.1 wt. % Cr_2O_3 and 24.1–37.0 wt. % Al_2O_3 contents (Table 1). Spinel in wehrlite and olivine websterite xenoliths has higher cr# (0.20–0.30) and lower mg# (0.66–0.70) than that in harzburgite and lherzolite xenoliths (0.12–0.15, 0.75–0.76, respectively) (Tables 1 and 2). Spinel from Type-II xeno-

liths shows a wide range in composition, whereas spinel from olivine websterites (BROI1) overlaps with that of the Type-I xenoliths (Table 2). In the KONGII1 clinopyroxenite spinel is between Type-I and the other two Type-II rocks, which show the lowest Cr_2O_3 and MgO content (Table 2). The spinel in olivine websterite (BROI1) is characterized by the highest Cr-value (cr#) of 0.30.

Feldspar

Feldspar as a primary phase is only found in the plagioclase-bearing ultramafic xenolith (KZSII4) of the Type-II series (Fig. 2f). The feldspar is labradorite and inhomogeneous in composition (Table 2). Its anorthite content ranges from 61 % to 68 %. However, feldspar as a secondary phase in interstitial glass of SISTI2b is enriched in Na, and has an anorthite content of 40–45 % (Table 1).

Glass

Glasses in the xenoliths from the NMD are plotted on the total alkalis vs. silica diagram (Table 1, Fig. 4) (Le Bas et al. 1986). Interstitial glass in the wehrlite and lherzolite xenoliths (SISTI2b and KZC1, respectively) display very high total alkalis and fall in the phonolite-tephriphonolite-trachyte field (note that these fields do not mean that these glasses correspond to any particular volcanic rock, since in this case it is not used for bulk composition of igneous rocks). However, this glass exhibits very high Al_2O_3 (23.3 wt. %) and very low CaO (0.77 wt. %) and MgO (0.82 wt. %) contents (Table 1). Glass in the spongy rim of orthopyroxene, displays a similarly high alkali content at an elevated SiO_2 content. Glass in the spongy rim of clinopyroxene shows the widest range of composition. The SiO_2 content varies between those of interstitial glass and glass in the spongy rim of orthopyroxene, whereas only the maximum alkali concentration of glass in the spongy rims of clinopyroxene is comparable to that of the former ones (Table 1, Fig. 4).

Trace element geochemistry of glass-bearing Type-I xenoliths

Representative *in situ* trace element analyses of clinopyroxenes (SISTI2b, KZC1, TLC1), orthopyroxenes (TLC1 and KZC1) and interstitial glasses (SISTI2b) from the melted Type-I peridotites and those of their host rock are reported in Table 1. Since the grain size of secondary minerals and glass patches in the rims of clinopyroxene and orthopyroxene are much smaller than the optimal smallest spot size of the LA-ICPMS, only bulk analyses were available from the spongy rims of these minerals (Fig. 2b,d).

Clinopyroxene

The cores of clinopyroxene (clear clinopyroxene without any interstitial glass) show different trace element patterns in the three different rock types (Fig. 5a–b). The overall REE pattern of clinopyroxene shows an enriched character (cf. C1 chondrite) with enrichment in LREE and depletion in HREE (Fig. 5a). Nevertheless, the SISTI2b wehrlite and TLC1 harzburgite have elevated MREE contents, whereas the KZC1 lherzolite shows convex upward REE pattern

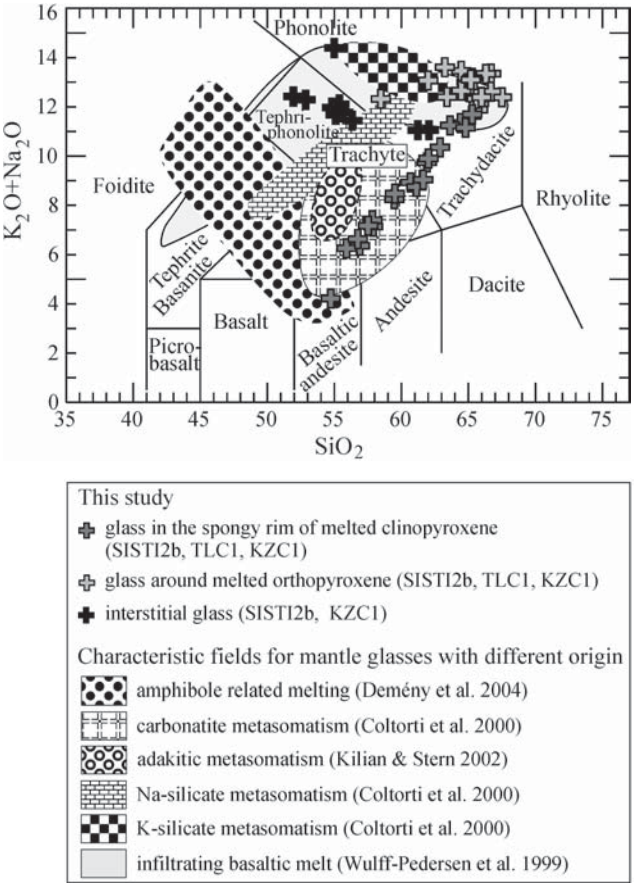

Fig. 4. Compositions of glass in ultramafic xenoliths from the North Minusinsk Depression plotted in the TAS diagram (Le Bas et al. 1986). Glass in lherzolite (KZC1) and harzburgite (TLC1) xenolith displays trachytic composition and is similar to those glasses related to incongruent melting of orthopyroxene. Glass in wehrlite (SISTI2b) exhibits lower SiO_2 and Na_2O+K_2O content than those in the harzburgite (TLC1) xenolith and falls into the phonolite-tephriphonolite field.

Fig. 5. Chondrite (Nakamura 1974) normalized REE and primitive mantle (McDonough & Sun 1988) normalized trace element distribution of clinopyroxene, orthopyroxene, glass and host basalt of the three selected North Minusinsk Depression xenoliths showing evidence of melting/metasomatism. Note that for better demonstration and understanding the log scale is not the same for clinopyroxene and orthopyroxene (a–d). Also, the shape of the symbol represents the rock type of the glasses (e–h). **(a)** — C1 chondrite normalized REE pattern of clinopyroxenes. **(b)** — Primitive mantle normalized trace element pattern of clinopyroxenes. **(c)** — C1 chondrite normalized REE pattern of orthopyroxenes. **(d)** — Primitive mantle normalized trace element pattern of orthopyroxenes. **(e)** — C1 chondrite normalized REE pattern of interstitial glass from SISTI2b wehrlite. **(f)** — Primitive mantle normalized trace element pattern of interstitial glass from SISTI2b wehrlite. **(g)** — C1 chondrite normalized REE pattern of glass from the host basalt. **(h)** — Primitive mantle normalized trace element pattern of glass from the host basalt.

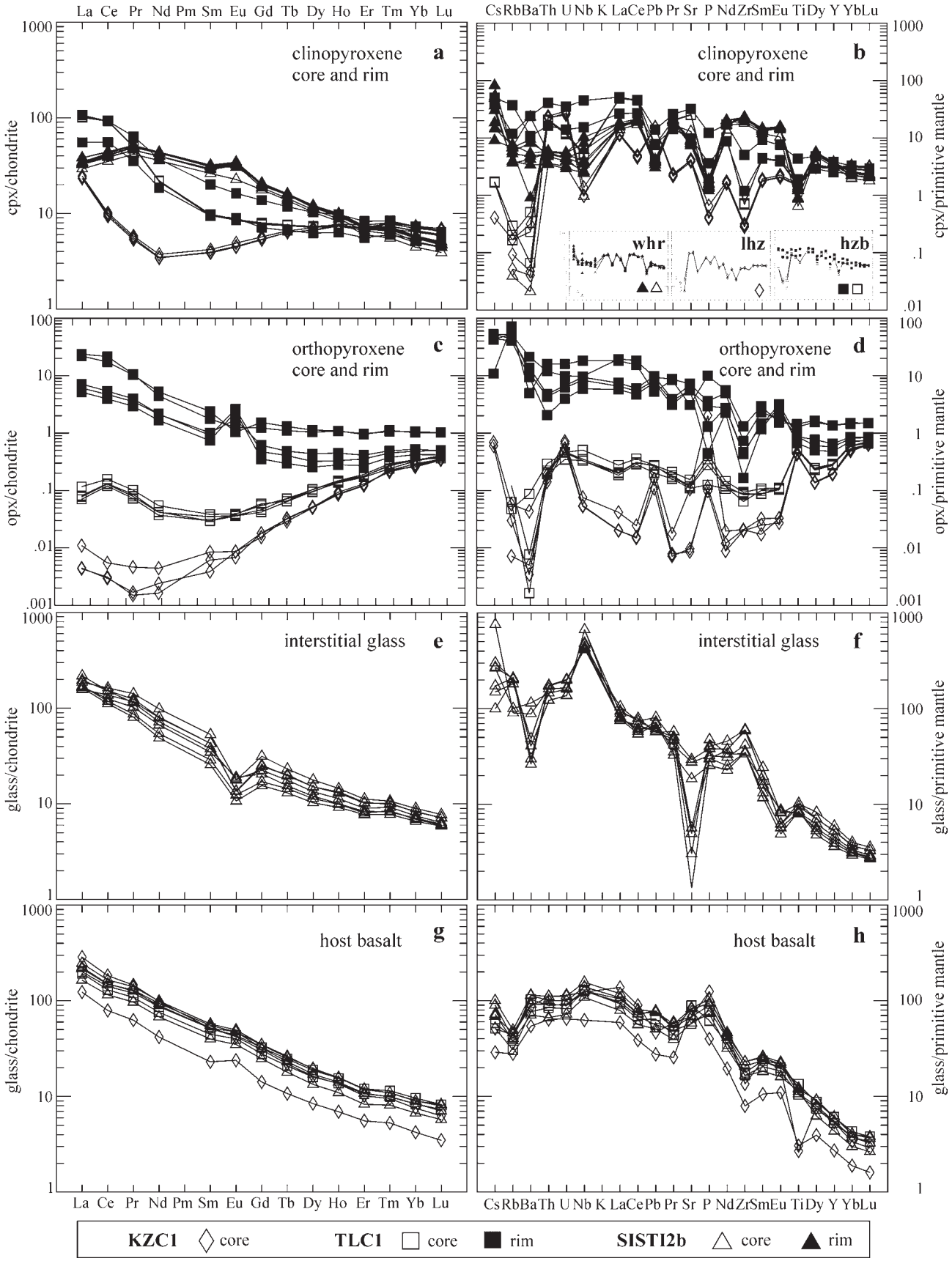
La Ce Pr Nd Pm Sm Eu Gd Tb Dy Ho Er Tm Yb Lu
Cs Rb Ba Th U Nb K La Ce Pb Pr Sr P Nd Zr Sm Eu Ti Dy Y Yb Lu
clinopyroxene core and rim
a
b
orthopyroxene core and rim
c
d
interstitial glass
e
f
host basalt
g
h
cpx/chondrite
cpx/primitive mantle
opx/chondrite
opx/primitive mantle
glass/chondrite
glass/primitive mantle
whr
lhz
hzb
KZC1 core
TLC1 core rim
SISTI2b core rim

Fig. 5.

with depletion in MREE. Spongy rims, which consist of glass and clinopyroxene, show REE patterns similar to the clean clinopyroxene cores. The rims of SISTI2b wehrlite display a slight positive Eu-anomaly (Fig. 5a).

The trace element pattern of clinopyroxene shows negative anomalies (cf. primitive mantle) in HFS- (especially Ti, Zr an Nb) and fluid mobile elements (especially Pb) (Fig. 5b). Clinopyroxene exhibits considerable negative anomaly in LIL elements (especially Cs, Rb and Ba). Spongy rims display very similar trace element pattern to cores, apart from being enriched at least 100 times in LIL elements over the clean clinopyroxene (Fig. 5b).

Orthopyroxene

The REE composition of orthopyroxene shows convex upward pattern with enrichment in La, Ce, and HREE and depletion in MREE (Fig. 5c). The rims of orthopyroxenes (including glass, fine-grained secondary olivine and secondary clinopyroxene, see Fig. 2d for details) in TLC1 harzburgite are much more enriched in REE (2–12 times that of the C1 chondrite) than the core (0.01–0.1 times that of the C1 chondrite) and also displays a slight positive Eu-anomaly (Fig. 5c).

The orthopyroxene of TLC1 harzburgite shows significantly lower trace element concentrations relative to clinopyroxene (0.01–1 times that of the primitive mantle), with depletion in LIL elements (especially Rb, Ba) and positive anomalies in P and Ti (Fig. 5d). The orthopyroxene in KZC1 lherzolite shows negative anomalies in Rb, Ba, Nb, K, La, Pr, Sr and significant positive anomalies in P, Ti and fluid mobile elements (note that the spongy rim of orthopyroxene consists also of secondary olivine, glass and secondary clinopyroxene, Fig. 2d). The orthopyroxene rims in TLC1 harzburgite are enriched in LIL (especially Cs, Rb) and slightly depleted in HFS (especially Zr, Ti) elements (cf. primitive mantle), however, the trace element concentration is higher than that of the core for each element (Fig. 5d).

Interstitial glass

Interstitial glass was only analysed for trace elements in the SISTI2b wehrlite, because other glass patches in KZC1 were too small for appropriate analysis. The interstitial glass shows a REE pattern (cf. C1 chondrite) enriched in LREE and relative depletion in HREE (Fig. 5e).

Interstitial glass shows enrichment in LIL (especially Cs, Rb, Th) and HFS (especially Nb, Zr, Ti) elements. Significant positive anomalies were found in Rb, Nb and Zr. Negative anomalies were observed in Ba, Sr, and Eu (Fig. 5f).

Host basalt

Host rock analyses were carried out using a large spot size (~180 μm) and analysing host basalts of which microphenocrysts were smaller than 50 μm. A SiO_2 content of 52 wt. % has been used as internal standard. The trace element compositions of the host rocks are very similar in all the three studied xenoliths (Fig. 5g–h, Table 1). The general patterns of the REE and trace elements of interstitial glass look similar to the host basalt, however, the main differences are the negative Rb anomaly, positive P anomaly and the absence of significant positive anomaly in Nb and Zr in the host rock, in addition a slight positive Eu-anomaly occurs in the host basalt (Fig. 5g–h).

P-T estimations

We calculated the equilibrium temperature for the Type-I xenoliths using the Ca-in-opx geothermometer of Brey & Kohler (1990). For this calculation cores of primary orthopyroxenes were used and we assumed that the equilibrium pressure of the xenoliths was 1.5 GPa. The equilibrium temperatures of xenoliths from the NMD fall in the range of 960–1050 °C. The two-pyroxene method of Brey & Kohler (1990) was also applied and it provided temperatures of 1010–1150 °C, which is higher than for the Ca-in-opx method. However, the two-pyroxene method generally overestimates the real temperature. Oxygen fugacity was calculated using the method of Ballhaus et al. (1990). The oxygen fugacity varies between FMQ –2 and 0.5 $\Delta\log(fO_2)$.

Primary clinopyroxenes in Type-II xenoliths fall in the field of granulite and garnet clinopyroxenite xenoliths on the Al^{IV}-Al^{VI} diagram (not shown), which implies pressure condition corresponding to the lower crust-uppermost mantle transition. Approximate pressure values for these xenoliths are obtained by using the technique of Nimis (1995). This method gives 1.2–1.4 GPa (approximately 42–49 km) for this group of xenoliths.

Discussion

Some implications for the lithospheric mantle beneath the NMD

According to the petrographic and geochemical features, the xenoliths studied can be divided into two major groups. Type-I xenoliths and BROI1 clinopyroxene-rich xenoliths comprise the first group. BROI1 olivine websterite belongs to this group because it displays similar compositions to those of Type-I (peridotite) xenoliths. The relationship between the Fo content in olivines and cr# in the coexisting spinel of the lherzolite xenoliths from the NMD is plotted on Fig. 6. Subvertical lines indicate the degree of partial melting after Jaques & Green (1980). Note that this method only works for lherzolite xenoliths with moderate Al_2O_3 and CaO content. Type-I xenoliths of the NMD display a degree of depletion less than 20 %, applying the diagram of Arai (1994) (Fig. 6).

Type-I xenoliths from the North Minusinsk Depression show a wide petrological variety from dunite to plagioclase-bearing ultramafic rock and also a considerable geochemical diversity in minerals of different xenoliths. A depletion event is clearly reflected in the major and trace element composition of the mineral constituents in some

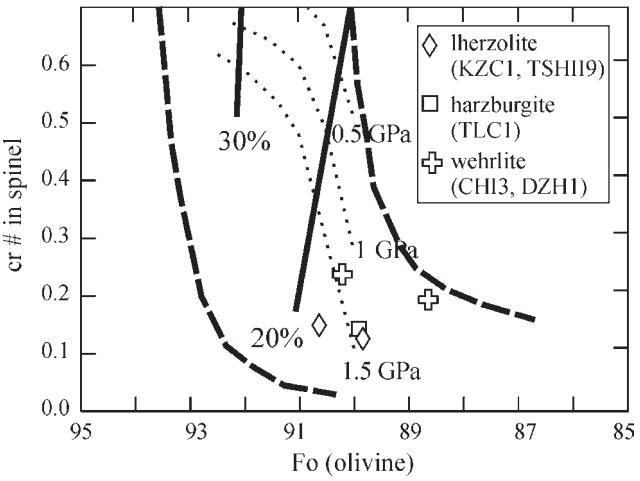

Fig. 6. Relationship between the Fo content of olivines and cr# = Cr/(Cr + Al) (in atomic ratio) of coexisting spinel in upper mantle xenoliths from the North Minusinsk Depression. OSMA = olivine-spinel mantle array is shown by dashed lines, after Arai (1994). The degree of partial melting is shown by subvertical lines (Arai 1994). Dotted lines indicate the approx. pressure of partial melting (Jaques & Green 1980).

xenoliths (original depletion in LREE subsequently overprinted by an enrichment process, high cr# and mg#). This depleted feature is documented in the composition of porphyroclastic pyroxenes and has been labelled "component A" by Frey & Green (1974). A subsequent enrichment is represented by a concave upward trace element pattern predominantly in rim of orthopyroxene and some clinopyroxene (i.e. enrichment in LREE (Fig. 5a,c)). This is called "component B" by Frey & Green (1974). Relatively low cr# in spinel and the fact that the suspected degree of partial melting is lower than 20 % (Tables 1, 2, Fig. 6) suggest that the continental lithosphere beneath the NMD is somewhat less depleted than those of areas with thinner lithosphere (i.e. Szabó et al. 2004). Seven relatively clinopyroxene-rich xenoliths are not enough to claim the less depleted nature of the lithosphere beneath this area. However, more than 100 xenoliths, from which these seven were selected for further study, display very similar modal composition based on macroscopic observations. The origin of clinopyroxene-rich (i.e. wehrlite such as SIST12b) xenoliths is commonly thought to be associated with carbonatite metasomatism (Yaxley et al. 1991). This is maybe supported by the trace element pattern of pyroxenes, which also shows enrichment in elements related to carbonatites (i.e. LREE, U, Th) (Yaxley et al. 1991) (Fig. 5a–d). Furthermore, Ionov et al. (2005) suggested that clinopyroxene enrichment in the mantle can also be achieved by interaction with silica undersaturated melts. The less depleted character of the lithosphere is in agreement with geological observations that there is no evidence for voluminous volcanic activity before the Cretaceous basaltic magmatism in the NMD, where only subordinate Devonian silicic volcanics have been reported. Therefore, the lack of extensive volcanism (Zubkov 1986; Zonenshain et al. 1990) in association with either the Cretaceous or the Devonian thinning events also prevented the continental lithospheric mantle of the NMD from a higher degree of depletion.

Clinopyroxenite and plagioclase-bearing ultramafic xenoliths (KONGII1, SISTII5, KZSII4) make up the Type-II group based on their comparable petrographic and geochemical characters. These rocks of the Minusinsk Region display high concentrations of basaltic major elements (i.e. Na, K, Al, Ca, Table 2) in the rock-forming minerals. In addition, the mineral assemblage in these xenoliths is enriched in clinopyroxenes and plagioclase. We suggest that these rocks crystallized from a basaltic melt close to the present day mantle/crust boundary beneath the North Minusinsk Depression (39–42 km) according to our pressure estimation. This likely indicates that the thickness of the crust has not changed considerably since the Cretaceous.

Melting and metasomatic phenomena

Textural evidence for melting

Three of the studied Type-I xenoliths display textural evidence of partial melting, which includes spongy rims of clinopyroxene and orthopyroxene, as well as interstitial glass. Interstitial glass in SISTI2b and KZC1 xenoliths shows no channels or connections towards the host basalt. Interstitial glass is in contact with the spongy rim of pyroxenes, which always contains glass. The extent of melting changes considerably from xenolith to xenolith. KZC1 lherzolite appears to be the least affected one as the modal proportion of the spongy rims of pyroxenes is small. The spongy rims are also too narrow to be analysed for trace elements. Tiny patches of interstitial glass, however, were observed in KZC1 lherzolite. TLC1 harzburgite exhibits transitional character with significant proportion of spongy rim but without interstitial glass. The melting process is most profound in the SISTI2b wehrlite, in which it is extremely difficult to find unmelted clinopyroxene and the modal proportion of interstitial glass is significant (2.4 v/v %, Table 1).

Closed or open system melting?

Under upper mantle conditions orthopyroxene melts incongruently mostly due to decreasing pressure and/or fluid flux. Incongruent melting of orthopyroxene forms Si-rich melt and olivine at the rims according to the equation of $opx_{core} = olivine + melt$ (e.g. Morse 1980; Tracy 1980). However, at the rims of melted orthopyroxene, beside the Si-rich glass and the olivine, secondary clinopyroxene was also observed (Fig. 2d). The presence of these newly formed clinopyroxenes cannot be explained solely by incongruent melting of orthopyroxene. Using mass balance calculation, the bulk major element composition of the spongy rim of the orthopyroxene can be estimated (proportion of olivine consistently 65 % area, glass 35 % area). This calculation gives excess in Al_2O_3, Na_2O and K_2O and deficit in CaO, Cr_2O_3 (MgO and FeO) for the spongy rim with respect to porphyroclastic orthopyroxene (Table 1). This observation suggests that melting is in-

duced by the addition of a metasomatic agent. The presence of newly formed clinopyroxenes in the incongruent rim of orthopyroxene is in agreement with metasomatic reactions (e.g. Coltorti et al. 2004). This hypothesis is further supported by the trace elements and REE's (Fig. 5c–d). The trace element and REE patterns show significant differences between the orthopyroxene cores and spongy rims in the TLC1 harzburgite. The cores show depleted character (0.01–1× of the primitive mantle), whereas the rims are enriched in fluid mobile and LIL elements and their concentrations are 3–100 fold higher than that of the primitive mantle. Furthermore, the cores are depleted in LREE, whereas the rims are enriched in LREE (Fig. 5c).

The melting of the clinopyroxenes under upper mantle conditions is a solid-solution controlled process (e.g. Golovin et al. 2000; Carpenter et al. 2002), where the primary clinopyroxene forms spongy rims, which contain melt accumulations (Fig. 2b). Similarly to orthopyroxene, the bulk major element composition of the melted part of the clinopyroxene can be determined by mass balance calculation. This is possible if the composition of the spongy rim and the enclosed glass, and their modal proportions are known. The precise proportions of the spongy rim including the glass were calculated using BSE images, which give consistently 82–88 % area for the spongy rim and 18–12 % area for the enclosed glass. If the melting event happened in a closed system then the calculated bulk composition of the spongy rims should be close to or the same as that of the core. This is not the case, because slight depletion in MgO, CaO, Cr_2O_3 (and FeO) and significant enrichment in Na_2O, K_2O and Al_2O_3 were observed within the spongy rims relative to the unaffected cores in the three xenoliths (KZC1 lherzolite, SISTI2b wehrlite and TLC1 harzburgite) (Table 1). The addition of a metasomatic agent is also supported by the trace element and REE pattern of the spongy clinopyroxenes, which show a slightly enriched character in LREE (Fig. 5a). This enrichment is less profound than in orthopyroxene because clinopyroxene contains a much higher amount of trace elements. Nevertheless, significantly higher amounts of fluid mobile elements are observed in the spongy rims of clinopyroxene than in the cores (Fig. 5b).

In summary, textural evidence, major and trace element composition all indicate that partial melting of clino- and orthopyroxene to produce the spongy rims did not occur in a closed system but was caused by the influx of an external (metasomatic?) agent.

Nature and composition of the metasomatic agent

The spongy rims of different pyroxenes display similar trace element and REE patterns (Fig. 5a–d), which suggests compositional similarities of the rims. Although the trace element compositions of the spongy rims of orthopyroxene represent a mixture of pyroxene, olivine and melt composition, the chemical similarity could be the result of a melting process, which seems to have been triggered by an agent enriched in LIL, LREE, fluid mobile elements and alkalis. All these features are also present in the host basalt and in the interstitial glass (Fig. 5e–h). We, therefore, need to evaluate whether either of these two melts was involved in the partial melting of the pyroxenes. No fractures or channels were seen where the host magma could have affected the chemical composition of the glasses inside the peridotites. The major element composition of the glass found within the spongy pyroxenes is characterized by very high Al_2O_3 and very low CaO contents and does not resemble the alkaline melt composition of the host basalt. The LILE pattern of the host basalts with a negative Rb anomaly is also different from the LILE patterns found in the spongy rims. As the most incompatible elements, such as LILE, are preferentially hosted in the melt the bulk analysis of the spongy rims of orthopyroxene and clinopyroxene provides a good approximation of the LILE composition of the glass found in these rims. Although there is a difference in major element chemical compositions in glass in rims around clinopyroxene and orthopyroxene, the general feature with high SiO_2 and very high Al_2O_3 is common (Table 1, Fig. 4). The LILE pattern of the interstitial melt also resembles the LILE pattern in the spongy rims, apart from Ba, which in some analyses of interstitial glass displays a negative anomaly. Combining our textural and chemical evidence, we suggest that the interstitial melt is an appropriate candidate for being either the residuum after the addition of an external metasomatic agent to the melting assemblage of orthopyroxene±clinopyroxene or the external component itself. It is unlikely that there was no interaction between the metasomatic agent and the melting assemblage, therefore the former assumption seems to be more feasible. In the following we will put constraints on the geochemistry and origin of the interstitial glass.

In order to characterize the metasomatic agent, we should also consider whether the quenching process, which led to the formation of the interstitial glass, had any impact on its composition as it was pointed out in earlier works (e.g. Wilkinson 1966; Frey & Green 1974). In our samples small feldspar and clinopyroxene crystals have been recognized in interstitial glass which is also in contact with the spongy rim of both orthopyroxene and clinopyroxene and olivine. In addition, no rims (i.e. other than spongy rim) or zones have been observed in minerals adjacent to the interstitial glass excluding the possibility of any overgrowth related to the crystallization of this glass. In conclusion, the composition of interstitial glass has been only modified by the crystallization of minor amount of feldspar and clinopyroxene. Especially, the crystallization of feldspar might explain the negative anomaly of Ba, Sr and Eu in some analyses of interstitial melt as feldspar preferentially incorporates these elements with respect to other trace elements of comparable compatibility.

At least four possible models have been proposed in the literature for the origin of interstitial glasses (as either the residuum after addition of a metasomatic agent to the melting assemblage of the mantle or the trapped metasomatic agent itself) in xenoliths from the upper mantle, which include: 1 — infiltration and reaction of the xenoliths with the host magmas during their transportation to

the surface (e.g. Wulff-Pedersen et al. 1999; Shaw & Klugel 2002), 2 — anhydrous or hydrous partial melting of upper mantle rocks during decompression and heating (e.g. Jaques & Green 1980; Doukhan et al. 1993), 3 — breakdown and melting of pre-existing hydrous phases (amphibole and phlogopite) owing to decompression and heating (e.g. Frey & Green 1974; Wilson & Downes 1991; Yaxley et al. 1997, 1999), and 4 — infiltration and reaction of metasomatic fluid/melts in the mantle prior to entrainment into the host magma (e.g. Ionov et al. 1994; Szabó et al. 1996; Coltorti et al. 2000; Bali et al. 2002; Demény et al. 2004), where the nature of the agents can be various, and may include: carbonatites (e.g. Yaxley et al. 1991; Wiechert et al. 1997; Coltorti et al. 2000), andesites and adakites (Szabó et al. 1996; Kilian & Stern 2002), Na-rich melt/fluid (e.g. Beccaluva et al. 2001; Coltorti et al. 2004) and K-rich melt/fluid (Xu et al. 1996; Coltorti et al. 2000). These latter two agents (i.e. K and Na alkali silicate melts/fluids) may be closely related to the host magma, representing either an earlier incipient stage of melting in the mantle that later provided the host melt (Schiano et al. 1992; Schiano & Clocchiatti 1994), or these melts/fluids can represent a late stage crystallization/differentiation product of an alkaline basaltic magma (Zajacz et al. 2007).

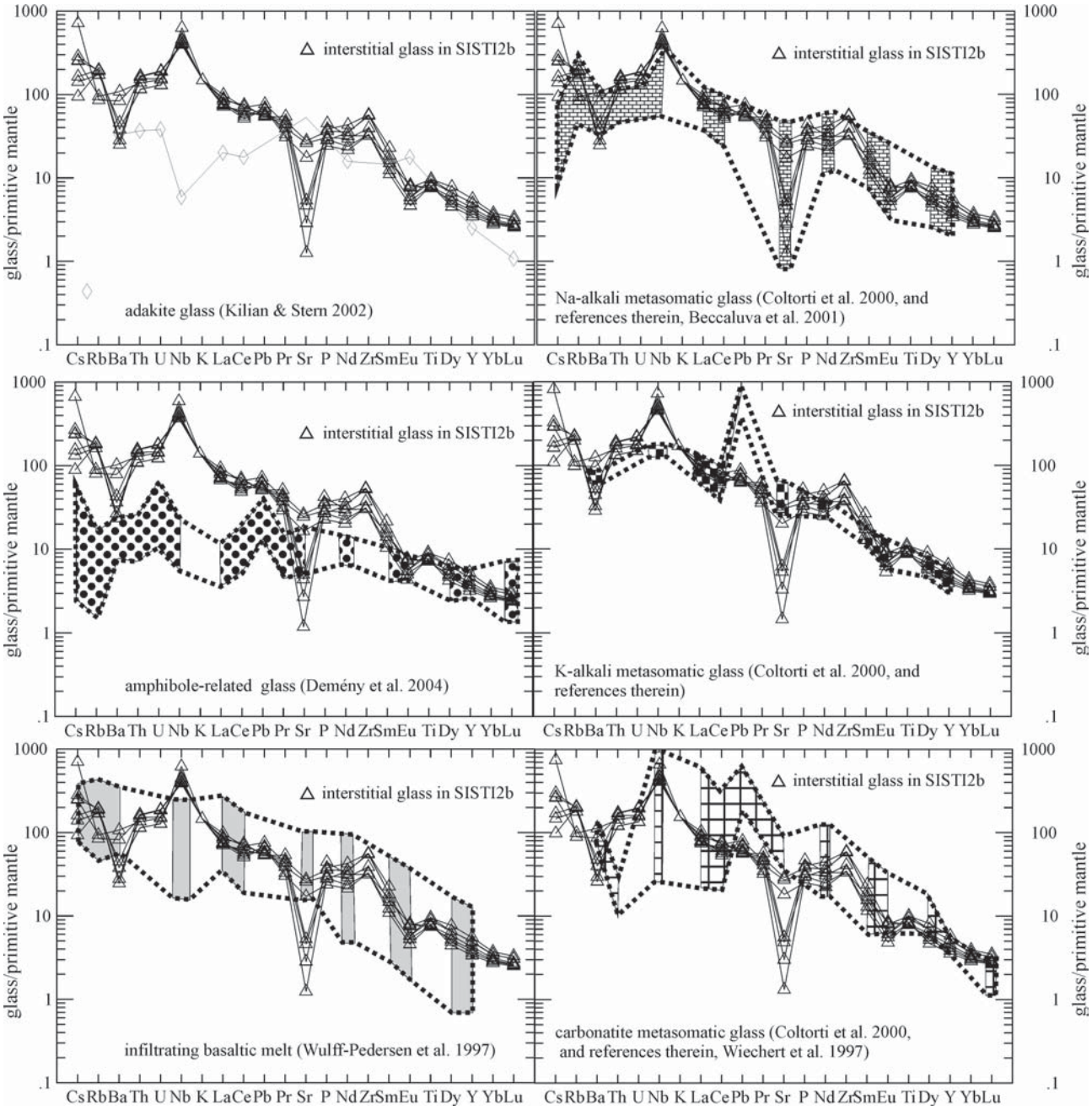

Fig. 7. Primitive mantle (McDonough & Sun 1988) normalized trace element pattern of mantle glasses with different origins compared to the studied glass in wehrlite SISTI2b from the North Minusinsk Depression.

As shown in the previous section, a simple *in situ* melting model cannot explain the excess of Na, Al, K in the rims of orthopyroxene and clinopyroxene because the rock forming minerals of the peridotites cannot produce such a considerable amount of Na, Al and K even if these major elements are highly incompatible. Hydrous phases have not been observed in the Type-I xenolith series of the NMD, therefore there is no direct evidence that breakdown of pre-existing hydrous phases during decompression and heating in a rising magma played a role. This theory is also not supported by the trace element composition of the interstitial glass, which is not similar to amphibole-related fluids/melts (Fig. 7, Demény et al. 2004). Consequently, an external source is suggested for the interacting agent(s). Textural and chemical evidence implies that not the host basalt but another melt was the source of the interstitial glass.

Origin of interstitial glass

The major element composition of interstitial glasses on the TAS diagram overlaps with the glasses of Wulff-Pedersen et al. (1999) and Coltorti et al. (2000), indicating either the infiltration of basaltic melt or a Na-K alkali metasomatism responsible for the formation of interstitial glass (Figs. 4, 8). Plotting the chemical composition of these interstitial glasses on a TiO_2+K_2O vs. $CaO+Na_2O$ discrimination diagram of Coltorti et al. (2000), they fall in the field depicted for Na-alkali silicate metasomatism, and only those in the KZC1 lherzolite are in the carbonatite field (Fig. 8). Primitive mantle normalized trace element patterns of different mantle glasses are compared to the studied interstitial glass in SISTI2b (Fig. 7). Subducted slab-related glass exhibits distinctive negative Nb- and positive Sr-anomaly, whereas amphibole-related glasses are considerably depleted (100 times) in LIL and LREE and in U, Th, Nb and K compared to the studied one. Carbonatite metasomatism formed glasses show a more or less similar pattern to the studied one, which is, however, more enriched in Th and depleted in Pb, Pr and Sr. K- and Na-alkali silicate metasomatism- and host basalt infiltration-related glasses display very similar patterns to the studied glass, the most similar one of which is the Na-alkali silicate metasomatism-related pattern. The former two cannot account for the observed positive Nb- and Cs-anomaly, whereas only the host basalt infiltration-related glasses can explain the positive Zr-anomaly. The Na-alkali silicate metasomatism-related, nonetheless, is in good agreement with all of these characteristic features of the interstitial glass in the SISTI2b xenolith. This is also in good agreement with our previous observations that melted rims of clinopyroxenes and orthopyroxenes show excess in Na, Al and K and also in LIL and LREE, which implies that there may be a link between the melted rims and the interstitial glasses. In this scenario the interstitial glass represents the residuum (interaction products) after melting induced by an external metasomatic agent at the rims of pyroxenes. We assume that a melt, which was enriched in incompatible major (especially Na, K, Al) and trace (especially fluid mobile and LIL) elements, had

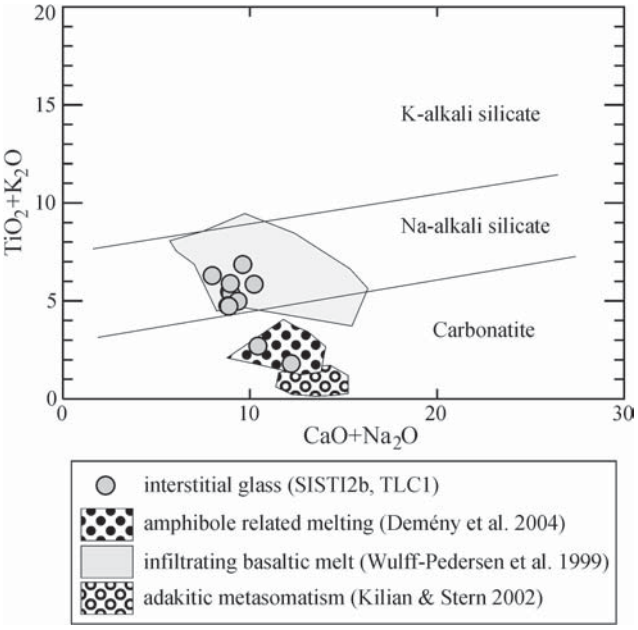

Fig. 8. $CaO+Na_2O$ vs. TiO_2+K_2O composition of glasses in the Type-I series (KZC1 lherzolite, SISTI2b wehrlite, TLC1 harzburgite) from the North Minusinsk Depression plotted on the discrimination the diagram of Coltorti et al. (2000), which is completed for the characteristic fields with data from Beccaluva et al. (2001) and Coltorti et al. (2004). Fields for adakite, amphibole and host basalt-related glasses are also indicated.

metasomatized the upper mantle prior to the transportation to the surface. This proposed alkali-rich silicate melt may be linked somehow to the host basalt, but their exact relationship is not yet known.

Evidence for earlier metasomatic events

Evidence for metasomatism prior to the studied melting event has been captured in the trace element composition of the pyroxenes. Orthopyroxene cores (TLC1, KZC1; Fig. 5c) display convex upward patterns with enrichment in La, Ce and Pr. In addition, clinopyroxene cores in KZC1 show a very similar pattern referring to a similar cryptic metasomatism (Fig. 5a). Enrichment in LREE over MREE and HREE in clinopyroxene cores is present in each analysed sample. We assume that the source of the cryptic metasomatism may have been either the Devonian volcanism or an earlier stage of the basaltic volcanism that brought up the xenoliths.

Concluding remarks

The studied Type-I xenoliths show variable degrees of depletion overprinted by an enrichment leading to LREE-enriched pyroxenes. The lithospheric mantle beneath the NMD appears to show a lower degree of depletion than other young areas with thinner lithosphere, which is in agreement with the lack of extensive volcanism in association with either the Cretaceous or Devonian thinning event, which prevented a higher degree of depletion of the

continental lithospheric mantle. Traces of extensive enrichment (e.g. presence of hydrous phases as amphibole and mica) are also absent. The studied Type-I xenoliths display equilibrium temperatures of 960–1050 °C. Type-II xenoliths of the NMD are the product of igneous crystallization in the subcontinental lithospheric mantle. This is confirmed both by the high content of basaltic elements in the constituent minerals and mineral assemblages of the studied xenoliths. They are probably equilibrated with their parental magma at 1.2–1.4 GPa (approximately 42–49 km), which is in good agreement with the present thickness of the crust beneath the NMD (39–42 km). This suggests that the thickness of the crust has not changed considerably since the Cretaceous.

The spongy rims of clinopyroxene containing glass, incongruent melting of orthopyroxene and interstitial glass provide evidence for incipient melting in the Type-I series of the NMD. We found enrichment in some major elements (especially Na, K, Al), fluid mobile- and LIL trace elements in rims of pyroxenes and interstitial glass, which cannot be explained solely by *in situ* melting of mantle silicates. Textural observations, coupled with major and trace element analysis, suggest that the interstitial glass is a residuum after a metasomatically-induced partial melting of pyroxenes. The melting was likely induced by a Na-alkali silicate melt/fluid. This melt/fluid is not the direct result of the host basalt infiltration, but it rather represents an earlier event, which could be in association with the basaltic volcanism that generated the host basalt.

Acknowledgments: The authors express their honor to Orlando Vaselli and †Filippo Olmi (University of Florence) for major element work. We are also grateful to György Falus (Lithosphere Fluid Research Lab, Eötvös University) for his helpful discussions. Members of the field team (J. Dégi, K. Kóthay, M. Pető, Z. Siklósy, Z. Zajacz) are acknowledged for their help in sample collection. The authors are grateful to Dmitri Ionov, Andy Beard, Marian Janák, an anonymous reviewer and Heather Sparks for their constructive criticism which substantially improved an earlier version of the manuscript. This work greatly benefited from the fruitful discussions with David H. Green. The Russian Academy of Sciences and Hungarian Academy of Sciences are thanked for financial support based on the Project #52. This work is partially supported by an A. E. Ringwood Memorial Scholarship and an Australian International Postgraduate Research Scholarship to I. Kovács. This is the 22nd publication of the Lithosphere Fluid Research Lab of the Department of Petrology and Geochemistry at Eötvös University, Budapest, Hungary.

References

Arai S. 1994: Compositional variation of olivine-chromian spinel in Mg-rich magmas as a guide to their residual spinel peridotites. *J. Volcanol. Geothermal Res.* 59, 4, 279–293.

Ashchepkov I.V., Kepezhinskas V.V., Malkovets V.G. & Ovchinnikow Y.I. 1995: Mantle xenoliths from the Meso-Cenozoic volcanic pipes of Khakasia. In: Sobolev N.V. (Ed.): *6th International Kimberlite Conference*. Siberian Branch, RAS, Novosibirsk, 39.

Bali E., Szabó C., Vaselli O. & Török K. 2002: Significance of silicate melt pockets in upper mantle xenoliths from the Bakony-Balaton Highland volcanic field, Western Hungary. *Lithos* 61, 1–2, 79–102.

Ballhaus C., Berry R.F. & Green D.H. 1990: Oxygen fugacity controls in the Earth's upper mantle. *Nature* 348, 6300, 437–440.

Beccaluva L., Bonadiman C., Coltorti M., Salvini L. & Siena F. 2001: Depletion events, nature of metasomatizing agent and timing of enrichment processes in lithospheric mantle xenoliths from the Veneto volcanic province. *J. Petrology* 42, 1, 173–187.

Bence A.E. & Albee A.L. 1968: Empirical correction factors for electron microanalysis of silicates and oxides. *J. Geol.* 76, 4, 382–396.

Brey G.P. & Kohler T. 1990: Geothermobarometry in 4-phase lherzolites 2. New thermobarometers, and practical assessment of existing thermobarometers. *J. Petrology* 31, 6, 1353–1378.

Carpenter R.L., Edgar A.D. & Thibault Y. 2002: Origin of spongy textures in clinopyroxene and spinel from mantle xenoliths, Hessian Depression, Germany. *Miner. Petrology* 74, 2–4, 149–162.

Coltorti M., Beccaluva L., Bonadiman C., Salvini L. & Siena F. 2000: Glasses in mantle xenoliths as geochemical indicators of metasomatic agents. *Earth Planet. Sci. Lett.* 183, 1–2, 303–320.

Coltorti M., Beccaluva L., Bonadiman C., Faccini B., Ntaflos T. & Siena F. 2004: Amphibole genesis via metasomatic reaction with clinopyroxene in mantle xenoliths from Victoria Land, Antarctica. *Lithos* 75, 1–2, 115–139.

Demény A., Vennemann T.W., Hegner E., Nagy G., Milton J.A., Embey-Isztin A., Homonnay Z. & Dobosi G. 2004: Trace element and C-O-Sr-Nd isotope evidence for subduction-related carbonate-silicate melts in mantle xenoliths (Pannonian Basin, Hungary). *Lithos* 75, 1–2, 89–113.

Doukhan N., Doukhan J.C., Ingrin J., Jaoul O. & Raterron P. 1993: Early partial melting in pyroxenes. *Amer. Mineralogist* 78, 11–12, 1246–1256.

Draper D.S. & Green T.H. 1997: P-T phase relations of silicic, alkaline, aluminous mantle-xenolith glasses under anhydrous and C-O-H fluid saturated conditions. *J. Petrology* 38, 1187–1224.

Frey F.A. & Green D.H. 1974: The mineralogy, geochemistry and origin of lherzolite inclusions in Victorian basanites. *Geochim. Cosmochim. Acta* 38, 1023–1059.

Frey F.A. & Prinz M. 1978: Ultramafic inclusions from San-Carlos, Arizona — petrologic and geochemical data bearing on their petrogenesis. *Earth Planet. Sci. Lett.* 38, 1, 129–176.

Golovin A.V., Sharygin V.V. & Malkovets V.G. 2000: Melt evolution during crystallization of basanites of the Bele pipe, Minusa Depression. *Russian Geol. Geophys.* 41, 1760–1782.

Ionov D.A., Hofmann A.W. & Shimizu N. 1994: Metasomatism-induced melting in mantle xenoliths from Mongolia. *J. Petrology* 35, 3, 753–785.

Ionov D.A., Bodinier J.L., Mukasa S.B. & Zanetti A. 2002: Mechanisms and sources of mantle metasomatism: major and trace element compositions of peridotite xenoliths from Spitsbergen in the context of numerical modeling. *J. Petrology* 43, 12, 2219–2259.

Ionov D.A., Chanefo I. & Bodinier J.L. 2005: Origin of Fe-rich lherzolites and wehrlites from Tok, SE Siberia by reactive melt percolation in refractory mantle peridotites. *Contr. Mineral. Petrology* 150, 335–353.

Jaques A.L. & Green D.H. 1980: Anhydrous melting of peridotite at 0–15 kb pressure and the genesis of tholeiitic basalts. *Contr. Mineral. Petrology* 73, 3, 287–310.

Khramov A.N. 1997: Rotation of the Siberian platform and its shear tectonics in the structure of the lithosphere of the Earth and earth-group planets. *Nauka Press*, 436–451.

Kilian R. & Stern C.R. 2002: Constraints on the interaction between

slab melts and the mantle wedge from adakitic glass in peridotite xenoliths. *Eur. J. Mineral.* 14, 1, 25–36.

Kryukov A.V. 1964: A new type of volcanic pipe on the southwest margin of the Siberian Platform. In: Volobuev M.I. (Ed.): Geology of the Siberian Platform southwest margin. *Nedra Press,* Moscow, 196–204.

Le Bas M.J., Lemaitre R.W., Streckeisen A. & Zanettin B. 1986: A chemical classification of volcanic-rocks based on the total alkali silica diagram. *J. Petrology* 27, 3, 745–750.

Litasov Y.D., Malkovets V.G., Litasov K.D., Agashev A.M. & Orihasi Y. 2002: Petrogenesis of basanites from volcanic pipes of North Minusinsk depression, geology, geochemistry and geophysics. *10th RFBR Science Conference*, Irkutsk, Russia, 343–345.

Luchitsky I.V. 1960: Volcanism and tectonics of the Devonian basins in the Minusinsk intermountane trough. *USSR Acad. Sci.*, Moscow, 1–276.

Malkovets V.G., Ionov D.A., Griffin W.L., O'Reilly S.Y., Pokhilenko N.P. & Litasov K.D. 1998: A P-T-composition cross-section of spinel and garnet facies lithospheric mantle in the Minusinsk region of the Siberian craton. *7th International Kimberlite Conference,* Cape Town, South Africa, 543–545.

Malkovets V.G., Ionov D.A., Agashev A., Litasov Y., Orihasi Y., O'Reilly S. & Griffin W. 2000: Structure and composition of the mantle beneath the Minusinsk region SW of the Siberian Craton: A Sr-Nd isotope and trace element study. *10th Annual Goldschmidt Conference,* Oxford, UK, 662–663.

Malkovets V.G., Litasov Y.D., Tavin A.V., Litasov K.D. & Taylor L.A. 2003: Volcanic pipes as clues to upper mantle petrogenesis: Mesozoic Ar-Ar dating of the Minusinsk basalts, South Siberia. *Int. Geol. Rev.* 45, 2, 133–142.

McDonough W.F. & Sun S.S. 1988: A primitive mantle composition from xenoliths. *Chem. Geol.* 70, 1–2, 12–12.

Morse S.A. 1980: Basalts and phase diagrams: An introduction to the quantitative use of phase diagrams in igneous petrology. *Springer Verlag,* New York, Berlin, Heidelberg, 1–245.

Nakamura N. 1974: Determination of REE, Ba, Fe, Mg, Na and K in carbonaceous and ordinary chondrites. *Geochim. Cosmochim. Acta* 38, 5, 757–775.

Nimis P. 1995: A clinopyroxene geobarometer for basaltic systems based on crystal-structure modeling. *Contr. Mineral. Petrology* 121, 2, 115–125.

Schiano P. & Clocchiatti R. 1994: Worldwide occurrence of silica-rich melts in sub-continental and sub-oceanic mantle minerals. *Nature* 368, 6472, 621–624.

Schiano P., Clocchiatti R. & Joron J.L. 1992: Melt and fluid inclusions in basalts and xenoliths from Tahaa-Island, Society Archipelago — evidence for a metasomatized upper mantle. *Earth Planet. Sci. Lett.* 111, 1, 69–82.

Shaw C.S.J. & Klugel A. 2002: The pressure and temperature conditions and timing of glass formation in mantle-derived xenoliths from Baarley, West Eifel, Germany: the case for amphibole breakdown, lava infiltration and mineral-melt reaction. *Miner. Petrology* 74, 2–4, 163–187.

Szabó Cs., Bodnar R.J. & Sobolev A.V. 1996: Metasomatism associated with subduction-related, volatile-rich silicate melt in the upper mantle beneath the Nógrád-Gömör Volcanic Field, northern Hungary/southern Slovakia: Evidence from silicate melt inclusions. *Eur. J. Mineralogy* 8, 881–899.

Szabó C., Falus G., Zajacz Z., Kovács I. & Bali E. 2004: Composition and evolution of lithosphere beneath the Carpathian-Pannonian Region: a review. *Tectonophysics* 393, 1–4, 119–137.

Tracy R.J. 1980: Petrology and genetic significance of an ultramafic xenolith suite from Tahiti. *Earth Planet. Sci. Lett.* 48, 1, 80–96.

Wiechert U., Ionov D.A. & Wedepohl K.H. 1997: Spinel peridotite xenoliths from the Atsagin-Dush volcano, Dariganga lava plateau, Mongolia: A record of partial melting and cryptic metasomatism in the upper mantle. *Contr. Mineral. Petrology* 126, 4, 345–364.

Wilkinson J.F.G. 1966: Residual glasses from some alkali basaltic magmas from New South Wales. *Mineral. Mag.* 35, 847–860.

Wilson M. & Downes H. 1991: Tertiary Quaternary extension-related alkaline magmatism in western and central-Europe. *J. Petrology* 32, 4, 811–849.

Wulff-Pedersen E., Neumann E.R., Vannucci R., Bottazzi P. & Ottolini L. 1999: Silicic melts produced by reaction between peridotite and infiltrating basaltic melts: ion probe data on glasses and minerals in veined xenoliths from La Palma, Canary Islands. *Contr. Mineral. Petrology* 137, 1–2, 59–82.

Xu Y.G., Mercier J.C.C., Lin C., Shi L., Menzies M.A., Ross J.V. & Harte B. 1996: K-rich glass-bearing wehrlite xenoliths from Yitong, northeastern China: Petrological and chemical evidence for mantle metasomatism. *Contr. Mineral. Petrology* 125, 4, 406–420.

Yaxley G.M. & Kamenitsky V. 1999: In situ origin for glass in mantle xenoliths from southeastern Australia: insights from trace element composition of glasses and metasomatic phases. *Earth Planet. Sci. Lett.* 172, 97–109.

Yaxley G.M., Crawford A.J. & Green D.H. 1991: Evidence for carbonatite metasomatism in spinel peridotite xenoliths from western Victoria, Australia. *Earth Planet. Sci. Lett.* 107, 305–317.

Yaxley G.M., Kamenitsky V., Green D.H. & Falloon T.J. 1997: Glasses in mantle xenoliths from western Victoria, Australia, and their relevance to mantle processes. *Earth Planet. Sci. Lett.* 148, 433–446.

Zajacz Z., Kovács I., Szabó C., Halter W. & Pettke T. 2007: Insights into the evolution of mafic alkaline melts crystallized in the uppermost lithospheric mantle of the Nógrád-Gömör volcanic filed (Northern Hungary): a melt inclusion study. *J. Petrology* 48, 5, 853–883.

Zonenshain L.P., Kuzmin D.V. & Natapov L.M. 1990: Geology of the USSR: A plate-tectonic synthesis. *Geodynamics Ser.* 21, 242.

Zubkov V.S. 1986: Comparing alkaline olivine basalts from the Minusinsk depression system and Baikal rift. In: Tauson L.V. (Ed.): Geochemistry of volcanic rocks for various geodynamic setting. *Nauka Press,* Novosibirsk, USSR, 112–133.